DYNAMIC TOMOGRAPHIC IMAGING OF THE SOLAR CORONA

Mark D. Butala[1], Richard A. Frazin[2], Yuguo Chen[3], and Farzad Kamalabadi[1]

Department of Electrical and Computer Engineering[1], Department of Statistics[3], University of Illinois, USA
Department of Atmospheric, Oceanic and Space Sciences, University of Michigan, USA

Overview

New developments in data assimilation and statistical estimation theory are necessary to characterize the transient phenomena responsible for space weather. We present a state-space model for the time-varying corona and measurements. State estimation methods may then be used to solve the resultant time-dependent inverse problem. However, such a formulation demands new state-estimation methods that scale well with problem size. We describe a Monte Carlo state estimation algorithm, the localized ensemble Kalman filter (LEnsKF), that results in dramatic reductions in computation for tomographic inverse problems, thus enabling data-assimilative models of the stellar atmosphere.

1 Forward Problem

Electron Density: The measured polarized light $y_i(\cdot)$ at time index i is related to the unknown electron density $x_i(\cdot)$ by

$$y_i(\boldsymbol{\theta}_i, \boldsymbol{s}) = C \int_{\mathbb{R}} dl\, H(\boldsymbol{s}, \boldsymbol{s} + l\boldsymbol{\theta}_i)\, x_i(\boldsymbol{s} + l\boldsymbol{\theta}_i) + v_i(\boldsymbol{\theta}_i, \boldsymbol{s}) \tag{1}$$

where $\boldsymbol{\theta}_i$ is the orientation of the observer relative to the Sun, $\boldsymbol{s}$ is the coordinate in the measurement plane, l is the distance along the line of sight, $H(\cdot)$ is a known scattering function [1] that encapsulates the Thomson scattering physics, and $v_i(\cdot)$ is instrument-dependent noise. Discretizing (1) results in the linear system

$$\boldsymbol{y}_i = \boldsymbol{\Sigma}_i\, \boldsymbol{\Lambda}\, \boldsymbol{x}_i + \boldsymbol{v}_i = \boldsymbol{H}_i\, \boldsymbol{x}_i + \boldsymbol{v}_i \tag{2}$$

where $\boldsymbol{y}_i \in \mathbb{R}^M$, $\boldsymbol{\Sigma}_i$ corresponds to line integrals, the diagonal matrix $\boldsymbol{\Lambda}$ is the spatially-dependent scattering potential, and $\boldsymbol{x}_i \in \mathbb{R}^N$. Note that N may be large, e.g., dividing the 3D solar atmosphere into $100 \times 100 \times 100$ voxels results in N^6!

Electron Temperature: The observed light at extreme ultraviolet wavelength λ is related to the density of electrons at a given temperature T by the following, where $\psi(\cdot)$ is the emission process:

$$y_i(\boldsymbol{\theta}_i, \boldsymbol{s}, \lambda) = C \int_{\mathbb{R}} dl \int_0^\infty dT\, \psi(\lambda, T)\, x_i(\boldsymbol{s} + l\boldsymbol{\theta}_i, T) + v(\boldsymbol{\theta}_i, \boldsymbol{s}, \lambda). \tag{3}$$

Discretizing (3) results in the following: ($\otimes$: Kronecker product)

$$\boldsymbol{y}_i = (\boldsymbol{T} \otimes \boldsymbol{\Sigma}_i)\, \boldsymbol{x}_i = \boldsymbol{H}_i\, \boldsymbol{x}_i + \boldsymbol{v}_i. \tag{4}$$

with $\boldsymbol{T}$ given by a plasma emission model such as CHIANTI [2].

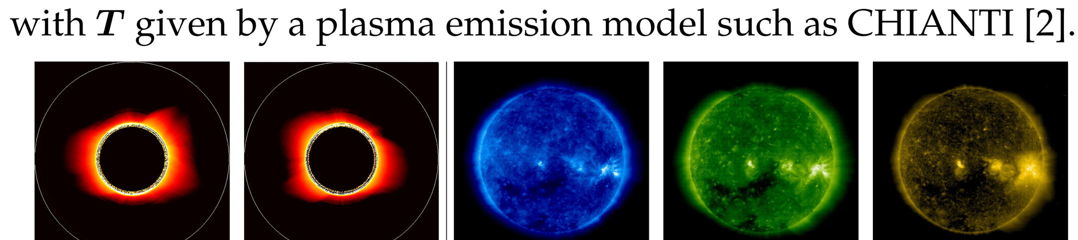

Mk4 2/11/08 | Mk4 2/18/08 | EIT 171 Å | EIT 195 Å | EIT 284 Å

2 Static Reconstruction

Prior work has assumed the unknown is fixed over $I = 14$ days

$$\boldsymbol{y}_{1:I} = \boldsymbol{H}_{1:I}\, \boldsymbol{x} + \boldsymbol{v}_{1:I} \tag{5}$$

where, e.g., $\boldsymbol{y}_{1:I} \triangleq (\boldsymbol{y}_1^T, \ldots, \boldsymbol{y}_I^T)^T$. Estimates may then be computed through a constrained, regularized optimization:

$$\widehat{\boldsymbol{x}} = \underset{\boldsymbol{x} \geq \boldsymbol{0}}{\arg\min}\, \|\boldsymbol{y}_{1:I} - \boldsymbol{H}_{1:I}\, \boldsymbol{x}\|_2^2 + \lambda \|\boldsymbol{D}\, \boldsymbol{x}\|_2^2. \tag{6}$$

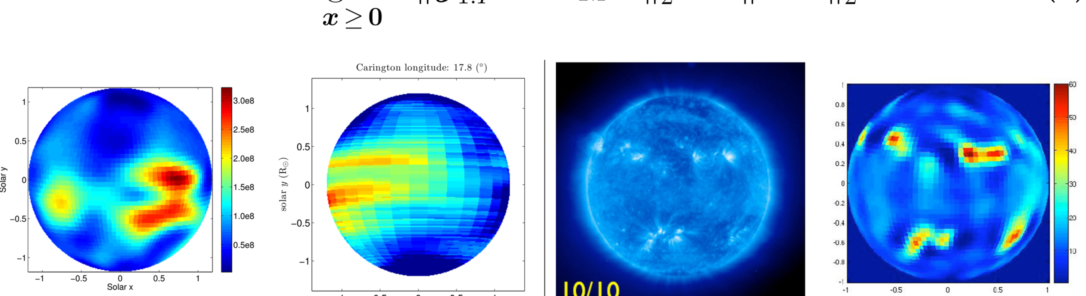

Density $\widehat{\boldsymbol{x}}$ | "Smearing" in static $\widehat{\boldsymbol{x}}$ | EIT 171 Å | Emissivity $\widehat{\boldsymbol{x}}$

3 Dynamic Reconstruction

Dynamic Signal Model:	General Hidden Markov	Linear Additive Noise
Initial prior:	$p(\boldsymbol{x}_1)$	$\boldsymbol{\mu} \triangleq \mathrm{E}[\boldsymbol{x}_1],\ \boldsymbol{\Pi}_1 = \mathrm{Var}(\boldsymbol{x}_1)$
Measurement model:	$h_i(\boldsymbol{y}_i \vert \boldsymbol{x}_i)$	$\boldsymbol{y}_i = \boldsymbol{H}_i \boldsymbol{x}_i + \boldsymbol{v}_i,\ \ \mathrm{Var}(\boldsymbol{v}_i) = \boldsymbol{R}_i$
State-transition model:	$f_i(\boldsymbol{x}_{i+1} \vert \boldsymbol{x}_i)$	$\boldsymbol{x}_{i+1} = \boldsymbol{F}_i \boldsymbol{x}_i + \boldsymbol{u}_i,\ \ \mathrm{Var}(\boldsymbol{u}_i) = \boldsymbol{Q}_i$

Under the above signal models, dynamic tomographic reconstructions may be computed as minimum mean square error (MMSE) state estimates: $\widehat{\boldsymbol{x}}^\star_{i|j} \triangleq \int_{\mathbb{R}^N} \boldsymbol{x}_i\, p(\boldsymbol{x}_i|\boldsymbol{y}_{1:i})\, d\boldsymbol{x}_i$. Each MMSE estimate $\widehat{\boldsymbol{x}}^\star_{i|j}$ is the optimal estimate of the N dimensional physical state $\boldsymbol{x}_i$ at time index i given the set of data $\boldsymbol{y}_{1:j} \triangleq \{\boldsymbol{y}_1, \ldots, \boldsymbol{y}_j\}$. It is in general computationally intractable to compute $\widehat{\boldsymbol{x}}^\star_{i|j}$ when the state dimension N is large.

3.1 Particle Filter (PF) [3]

The PF processes the set of particles $\{(w_i^l, \boldsymbol{x}_{i|j}^l)\}_{l=1}^L$ such that their empirical distribution converges to the posterior $p(\boldsymbol{x}_i|\boldsymbol{y}_{1:j})$ as the # of particles $L \to \infty$.

The PF estimates $\overline{\boldsymbol{x}}_{i|j}$ converge to the MMSE estimates $\widehat{\boldsymbol{x}}^\star_{i|j}$.

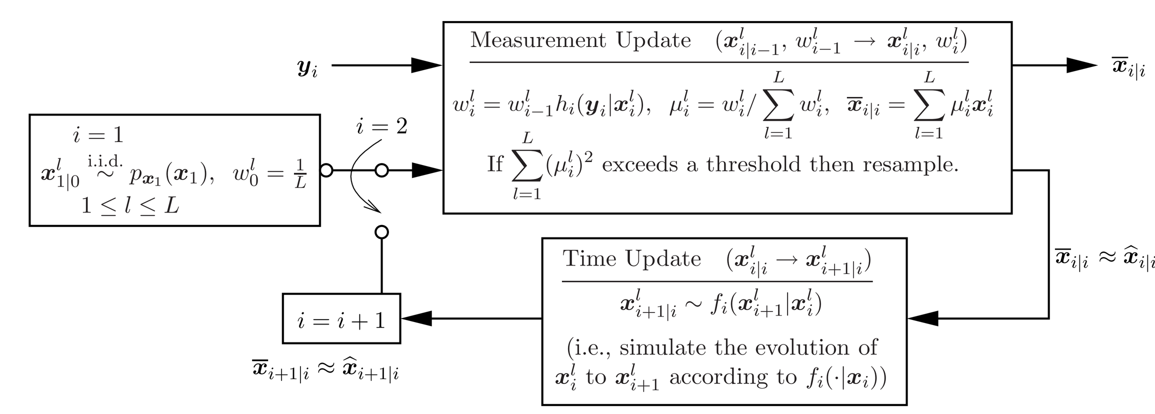

+: Operates under the general hidden Markov model, i.e., nonlinear problems.
−: Computationally limited to state dimensions no greater than $N \approx 100$, e.g., [3], [4].

3.2 Kalman Filter (KF) [5]

The KF computes linear MMSE (LMMSE) state estimates $\widehat{\boldsymbol{x}}_{i|j}$ which are MMSE optimal under the constraint that they must be an affine function of the data $\boldsymbol{y}_{1:j}$.

The KF is a deterministic algorithm while the PF and LEnsKF are Monte-Carlo algorithms.

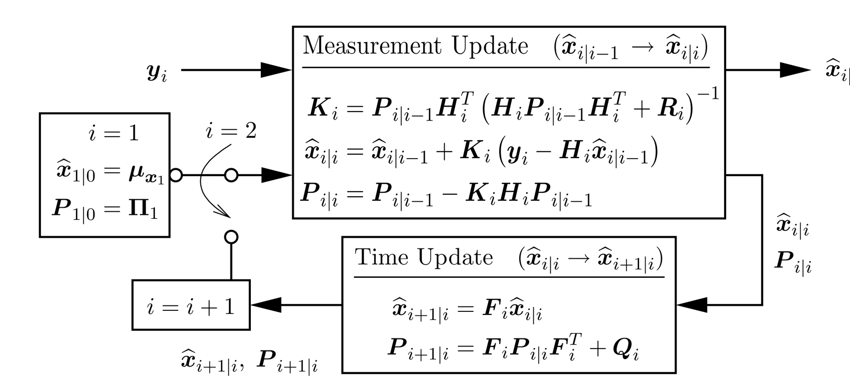

−: Requires the storage and operation on a massive matrix, i.e., $\boldsymbol{P}_{i|j}$ requires 2 TB of storage when $N = 10^6$.

3.3 Localized Ensemble Kalman Filter (LEnsKF) [6]

The LEnsKF processes an ensemble $\{\boldsymbol{x}^l_{i|j}\}_{l=1}^L$ such that the sample mean ($\widetilde{\boldsymbol{x}}_{i|j}$) and covariance ($\widetilde{\boldsymbol{P}}_{i|j}$) approximate the KF $\widehat{\boldsymbol{x}}_{i|j}$ and $\boldsymbol{P}_{i|j}$.

$\boldsymbol{C}_i \circ \widetilde{\boldsymbol{P}}_{i|j}$ is the localized estimate of $\boldsymbol{P}_{i|j}$. ($\circ$: the element-by-element matrix product)

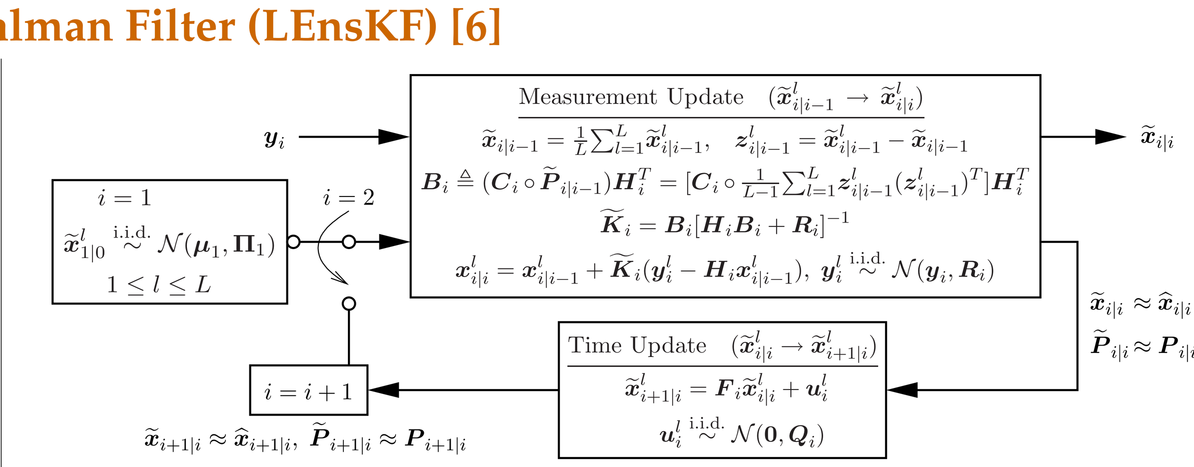

+: Computationally tractable for huge state dimension N applications when tapering is applicable.

4 Covariance Tapering

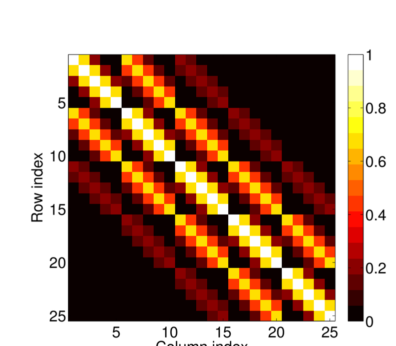

- The LEnsKF is computationally tractable only if the the ensemble size L is small.
- The sample covariance $\widetilde{\boldsymbol{P}}_{i|i-1}$ is a provably poor estimator of $\boldsymbol{P}_{i|i-1}$ when L is small. The LEnsKF instead uses $\boldsymbol{C}_i \circ \widetilde{\boldsymbol{P}}_{i|i-1}$ as the estimator of $\boldsymbol{P}_{i|i-1}$ [7].
- For typical problems, error correlations are strongest amongst spatial neighbors. The example taper matrix $\boldsymbol{C}_i$ (left) enforces this intuition where the (m, n)th element is close to 1 near the diagonal and 0 when far away.
- Covariance tapering introduces a bias but can greatly reduce the estimator variance. Ultimately, the proper choice of taper matrix enables a reduction in ensemble size L, many additional computational simplifications as a result of the sparsity of $\boldsymbol{C}_i$, and preserves a positive definite covariance matrix estimate.

5 Numerical Experiment

The performance of the LEnsKF is demonstrated in the following tomography simulation. The N dimensional unknown $\boldsymbol{x}_i$ is a highly dynamic random process with complicated motion, where the time index $1 \leq i \leq I$. Both a low and high sampling of the process are considered. The measurements $\boldsymbol{y}_i$ are a set of M parallel line integrals of $\boldsymbol{x}_i$ at some angle θ_i with 1% additive white Gaussian noise. The state transition model is $\boldsymbol{F}_i = \boldsymbol{I}$, i.e., the state evolution is modeled as a random walk. More sophisticated models may be easily incorporated.

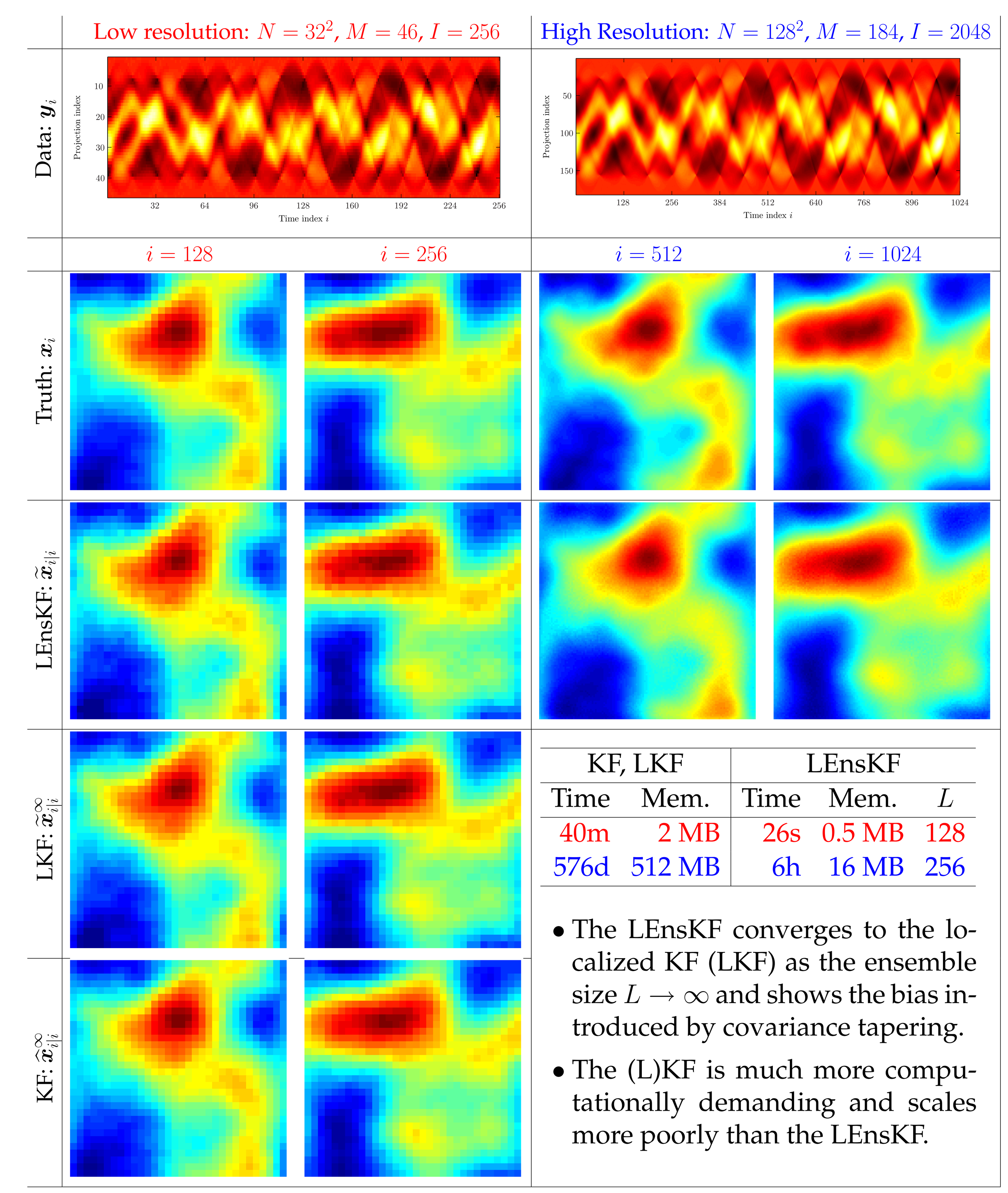

KF, LKF		LEnsKF		
Time	Mem.	Time	Mem.	L
40m	2 MB	26s	0.5 MB	128
576d	512 MB	6h	16 MB	256

- The LEnsKF converges to the localized KF (LKF) as the ensemble size $L \to \infty$ and shows the bias introduced by covariance tapering.
- The (L)KF is much more computationally demanding and scales more poorly than the LEnsKF.

6 Conclusions

The LEnsKF shows great promise for dynamic tomography applications as demonstrated in the numerical experiment. Scaling the method up for 4D solar tomography will require further developments. Fortunately, the method lends itself to parallelization, an endeavor that shows great preliminary promise.

References

[1] H. C. van de Hulst, "The electron density of the solar corona," *Bull. Astron. Inst. Netherlands*, vol. 11, no. 410, pp. 135–150, 1950.

[2] E. Landi, G. Del Zanna, P. R. Young, K. P. Dere, H. E. Mason, and M. Landini, "CHIANTI - an atomic database for emission lines - VII. New data for X-rays and other improvements," *Astrophys. J. Suppl.*, vol. 162, pp. 261–280, 2006.

[3] A. Doucet, N. de Freitas, and N. Gordon, Eds., *Sequential Monte Carlo Methods in Practice*. New York, NY: Springer-Verlag, 2001.

[4] F. Daum and J. Huang, "Curse of dimensionality and particle filters," in *Proc. IEEE Aerospace Conf.*, vol. 4, Big Sky, Montana, 2003, pp. 1979–1993.

[5] B. D. O. Anderson and J. B. Moore, *Optimal Filtering*. Englewood Cliffs, New Jersey: Prentice-Hall, 1979.

[6] G. Evensen, "Sequential data assimilation with a nonlinear quasi-geostrophic model using Monte Carlo methods to forecast error statistics," *J. Geophys. Res.*, vol. 99, pp. 10 143–10 162, 1994.

[7] P. L. Houtekamer and H. L. Mitchell, "A sequential ensemble Kalman filter for atmospheric data assimilation," *Mon. Weather Rev.*, vol. 129, pp. 123–137, 2001.